# Growth of large single-crystalline two-dimensional boron nitride hexagons on electropolished copper

Tay, Roland Yingjie; Griep, Mark H.; Mallick, Govind; Tsang, Siu Hon; Singh, Ram Sevak; Tumlin, Travis; Teo, Edwin Hang Tong; Karna, Shashi P.

2014

Tay, R. Y., Griep, M. H., Mallick, G., Tsang, S. H., Singh, R. S., Tumlin, T., Teo, E. H. T., & Karna, S. P. (2014). Growth of Large Single-Crystalline Two-Dimensional Boron Nitride Hexagons on Electropolished Copper. Nano Letters, 14(2), 839-846.

https://hdl.handle.net/10356/103803

https://doi.org/10.1021/nl404207f

# Growth of large single-crystalline two-dimensional boron nitride hexagons on electropolished copper

Roland Yingjie Tay,[†,‡] Mark H. Griep,[§] Govind Mallick,[‡,§] Siu Hon Tsang,[‡] Ram Sevak Singh,[†] Travis Tumlin,[§] Edwin Hang Tong Teo,[†,∥,*] and Shashi P. Karna[§]

[†]School of Electrical and Electronic Engineering, Nanyang Technological University, 50 Nanyang Avenue, Singapore 639798, Singapore

[‡]Temasek Laboratories@NTU, 50 Nanyang Avenue, Singapore 639798, Singapore

[§]Weapons and Materials Research Directorate, U.S. Army Research Laboratory, Aberdeen Proving Ground, MD, 21005, USA

[∥]School of Materials Science and Engineering, Nanyang Technological University, 50 Nanyang Avenue, Singapore 639798, Singapore

**ABSTRACT**

Hexagonal-boron nitride (h-BN) or 'white graphene' has many outstanding properties including high thermal conductivity, high mechanical strength, chemical inertness, and high electrical resistance, which open up a wide range of applications such as thermal interface material (TIM), protective coatings, and dielectric in nanoelectronics which easily exceed the current advertised benefits pertaining to the graphene based applications. The development of h-BN films using chemical vapour deposition (CVD) has thus far led into nucleation of triangular or asymmetric diamond shapes on different metallic surfaces. Additionally, the average size of the triangular domains has remained relatively small (~0.5 $\mu m^2$) leading to a large number of grain boundaries and defects. While the morphology of Cu surfaces for CVD-grown graphene may have impacts on the nucleation density, domain sizes, thickness, and uniformity the effects of the decreased roughness of Cu surface to develop h-BN films are unknown. Here, we report the growth and characterization of novel large area h-BN hexagons using highly electropolished Cu substrate under atmospheric pressure (AP) CVD conditions. We found that the nucleation density of h-BN is significantly reduced while domain sizes increase. In this study, the largest hexagonal-shape h-BN domain observed is 35 $\mu m^2$ which is an order of magnitude larger than a typical triangular domain. As the domains coalesce to form a continuous film, the larger grain size offers a more pristine and smoother film with lesser grain boundaries induced defects.

TOC graphic:

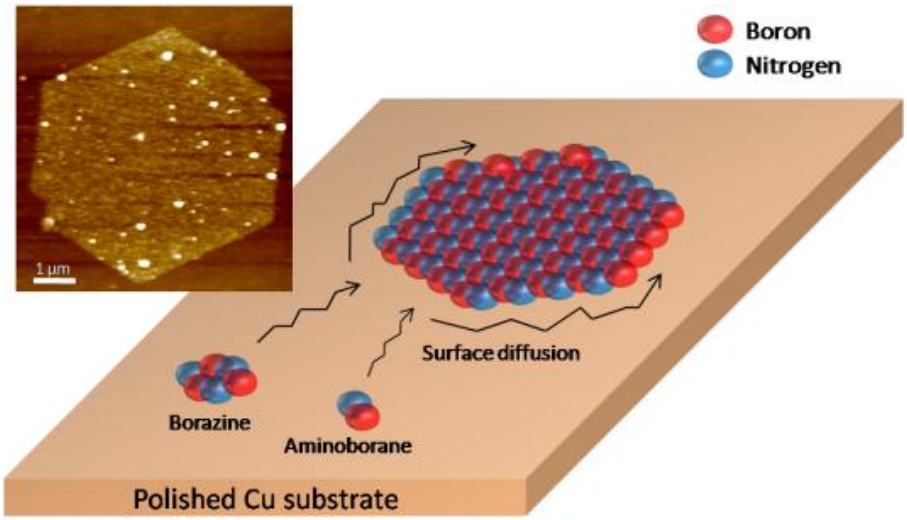


KEYWORDS: hexagonal boron nitride, atmospheric pressure chemical vapour deposition, scanning electron microscopy, atomic force microscopy.

Two-dimensional (2D) hexagonal-boron nitride (h-BN) and graphene are mono-layers of their layered counterparts, namely bulk h-BN and graphite, respectively. They both have very similar properties ranging from high thermal conductivity (h-BN ~1700-2000 W $mK^{-1}$, graphene ~2500-5000 W $mK^{-1}$),[1, 2] to high mechanical strength and hardness (breaking strength of 15.7 and 42 N $m^{-1}$, and elastic constant of 503 and 340 N $m^{-1}$ for h-BN and graphene, respectively)[3, 4] with almost matching lattice constant differing only by ~2% from each other. However, despite such similarities, their different chemical composition results in large contrast in electronic properties. For example, h-BN is a dielectric with a high electrical resistance and a wide bandgap of 6 eV,[5] while graphene is a semi-metal with zero bandgap and an extremely high carrier mobility (~10,000 $cm^2$ $V^{-1}.s^{-1}$).[6, 7] Therefore, these materials perfectly complement each other for nanoscale metal-insulator – based device applications. Recent experiments have shown that by patterning both materials, heterostructures of ultra-thin in-plane circuitry can be made.[8, 9] The close lattice matching, atomic-scale smoothness and absence of dangling bonds also make them excellent pairing materials with the mobility in graphene enhanced by an order of magnitude when h-BN is used as substrate layer, as compared to conventional $SiO_2$ substrates.[10, 11] Recently, h-BN showed high potential to be used as dielectric material for high-performance graphene devices with a wide range of capabilities ranging from radio frequency (RF) applications,[12] field-effect tunnelling transistors,[13] to capacitors.[14] Other properties known exclusively for h-BN is its ability to stay chemically inert and stable at high temperature of up to 1000 °C.[15] All these outstanding properties made h-BN uniquely suitable for a wide range of applications as dielectric material for flexible nanoelectronics,[16] ultraviolet (UV) lasing material,[5, 17] top based thermal interface material (TIM),[18] protective coatings,[19, 20] as well as for water purification and treatment.[21]

Chemical vapor deposition (CVD) has recently emerged as a technique for large scale growth of controllable h-BN thin films by both atmospheric pressure (AP) and low pressure (LP) CVD using Cu,[3, 11, 22-25] Ni,[24, 26] and Pt[27, 28] as catalytic substrates. The h-BN domains in these films tend to nucleate in triangular[22, 23, 27] or asymmetric diamond shape.[22] Although full film coverage consisting of multiple

overlapping domains is possible, the small average size of these domains (~0.5 $\mu m^2$) leads to large number of grain boundaries and defects.[29] These small domain sizes also hamper direct studies of single crystalline h-BN requiring domains in the range of at least micrometers. Contrasting with h-BN, extensive work has been done on graphene to increase the grain size with dimensions achieving upwards of millimeter in scale.[30, 31] This can be achieved through careful control of the surface morphology of the substrate used and other growth conditions. The nucleation density, domain sizes, thickness, uniformity and quality of CVD-grown graphene film,[32-34] can all be controlled this way. Moreover, a variety of different domain shapes such as hexagons,[30, 31, 34-36] squares,[37] rectangles[38, 39] polygons,[40] and four/six lobes flowers[41] are synthesized by catalytic CVD growth on Cu. An experimental and theoretical studies by Meca et al.[42] presents the existence various range of shapes and evolution of graphene domains which are dependent on its growing edge energies, kinetics of edge attachment, and the role of Cu surface orientations. Most recently, Hao et al. showed that oxygen in the Cu surface plays a far more important role in achieving large graphene domains.[43]

CVD-grown h-BN on Cu substrate is expected to exist in various shapes, and have a similar correlation towards substrate roughness. Although hexagonal-shape BN ribbons (BNR) using hybrid type structures (using hexagonal-shape graphene domains as templates) have been reported[44] together with hexagonal-shape BN nanoplates,[45, 46] pure large domain 2D hexagonal-shape h-BN remains elusive. In fact, it is predicted that the growth only tend towards triangular shapes due to the asymmetric N and B-terminated edge energies.[47] Here we demonstrate the growth of hexagonal-shape h-BN through highly smoothened Cu surface achieved by electropolishing. The growth strategies and characterization of large and pristine 2D hexagonal-shape h-BN domains with domain sizes measuring up to of 35 $\mu m^2$ (exceeding the sizes of typical triangular domains by at least one order of magnitude) are also discussed.

We have recently developed a method of synthesizing controllable triangular-shape h-BN domains on Cu substrates by using APCVD, and showed the important effects of substrate position governing the gradual evolution of h-BN film coverage.[25] Figure 1 shows the enhancement of surface

smoothness by electropolishing the rough and deep parallel grooves[48] of commercially available Cu foil (Alfa Aesar). The effective polished area measures (3 × 1.67) $cm^2$ (Figure 1b). Significant improvement on the surface roughness is evident as revealed by optical images and AFM measurements performed on both the polished and unpolished Cu (Figure 1c-f). Using the same APCVD technique we used highly smoothened Cu substrates with RMS roughness, $R_q$, of 4.42 nm (Figure 1f), as compared to an as-purchased Cu foil, $R_q$ of 314.12 nm (Figure 1e), scanned within an area of (10 × 10) $\mu m^2$. Here, we observed that the as-grown h-BN domains are hexagonal instead of the usual triangular which, to the best of our knowledge, have never been reported before. The CVD growth of h-BN was carried out simultaneously on both polished and unpolished Cu foils (the polished and unpolished Cu foils were placed alongside) in order to evaluate the differences by undergoing the exact same conditions and parameters. With a growth temperature fixed at 1050 °C the amount of ammonia borane was restricted to 5 mg and heated at 60 °C. The growth was quenched after 10 min. Figure 2a,b shows the scanning electron microscopy (SEM) images of the as-grown h-BN on unpolished and polished Cu substrates, respectively. It is intriguing to note the contrasting difference between the nucleation patterns of h-BN on different Cu surfaces. Larger hexagonal domains are observed on the polished Cu substrates with an average size of 0.81 $\mu m^2$, as compared to triangular domains with an average size of 0.40 $\mu m^2$ on unpolished Cu. Clearly all the hexagonal domains are uniform throughout the polished Cu foil, indicating that they are single crystalline and not coalesced triangular domains. Additionally, the nucleation density significantly reduces from 1.04 × $10^6$ nuclei $mm^{-2}$ on unpolished surface to 3.6 × $10^5$ nuclei $mm^{-2}$ on smoother polished surface with h-BN domains more evenly spread. Parallel strips of high density nucleation of ~3 to 4 μm apart are seen on unpolished Cu due to the uneven grooves of the Cu surface which are active nucleation sites.[22] In order to achieve large domain sizes it is important to suppress the amount of nucleation sites as a hexagonal structure provides a larger dimension compared to a triangle. Here, we demonstrate that a highly smoothened surface is able to fulfil these requirements.

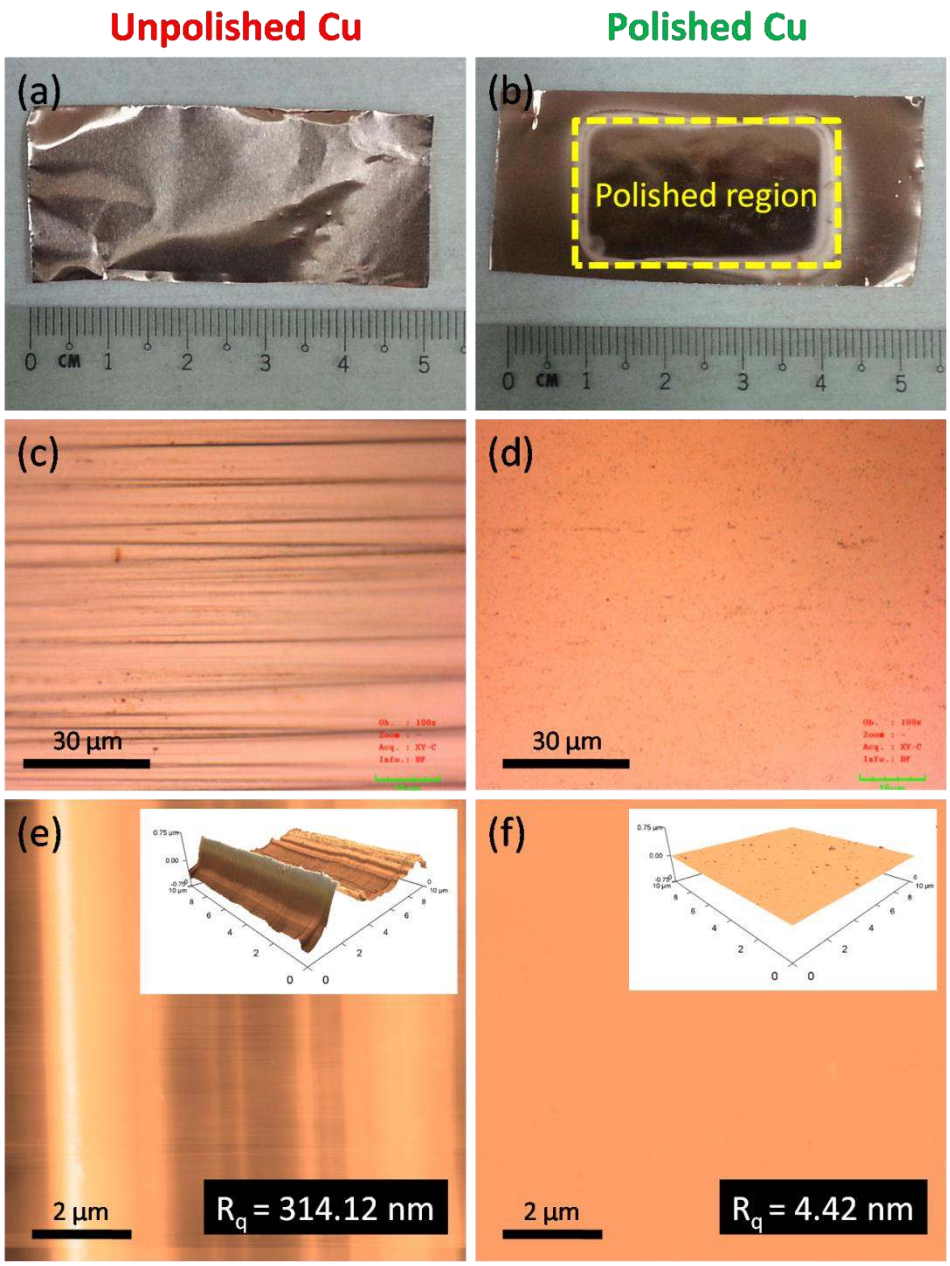


**Figure 1.** Cu surface roughness enhancement by electropolishing. Photographs and optical micrographs of an (a,c) unpolished Cu foil, and (b,d) polished Cu foil after 90 s of polishing time, respectively. AFM images with corresponding RMS surface roughness, $R_q$, of 314.12 nm and 4.42 nm of (e) unpolished (f) polished Cu foils, respectively. The inset of each figure shows the 3D height profile of the AFM scanned in (e) and (f), respectively.

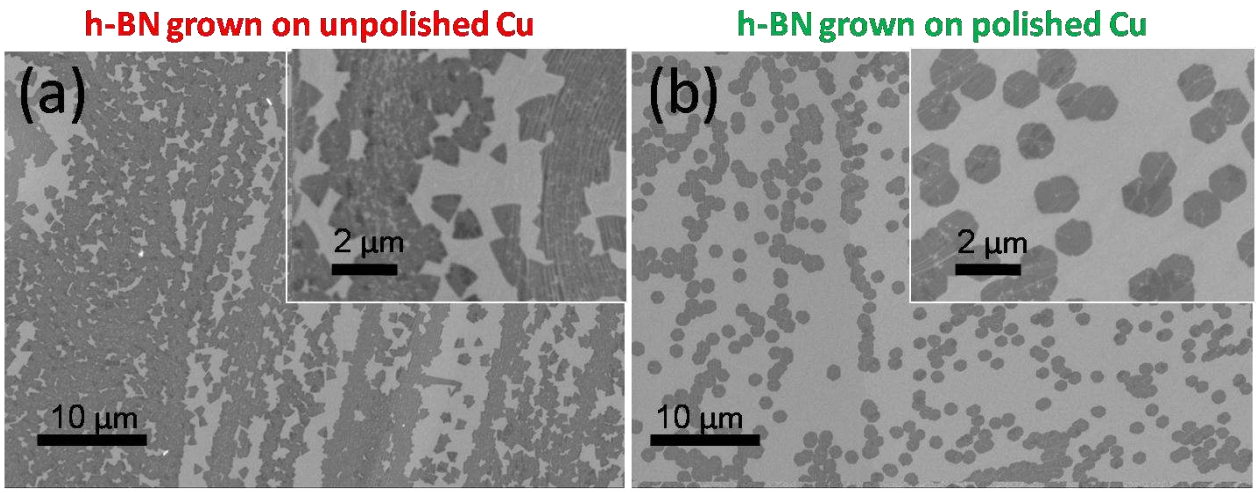


**Figure 2.** Dependence of Cu surface morphology on as-grown h-BN domains. SEM images of (a) triangular, (b) hexagonal-shape h-BN domains grown on unpolished and polished Cu, respectively. The inset in each figure shows higher magnification.

Further optimization of the process gives us the opportunity of achieving larger domain sizes. Thermal decomposition rate of the precursor, polymeric aminoborane into borazine ($B_3H_6N_3$) and aminoborane ($BH_2NH_2$)[49, 50] increases with small increase of temperature. While increased decomposition rate of polymeric aminoborane generally leads to increased "nucleation" of h-BN on surface with high roughness, the smooth surface of polished Cu impedes the rate of nucleation allowing for increase in the growth rate of the domain sizes. Under these assumptions, we used an elevated temperature of 65 °C to heat the precursor, increase the growth duration to 30 min, and position the substrates in the CVD reactor to achieve maximal film coverage ranging from sporadic h-BN domains to a continuous sheet. As the polished Cu foil has a length of ~3 cm, the foil was cut into half (parallel to its length), and placed in series (length-to-length alignment) in the quartz tube, to achieve an effective range of 6 cm for measurements (see Supporting Information Figure S1). Figure 3a-d shows the SEM images of the different stages of growth for a full coverage h-BN film on a highly polished Cu substrate. Each image is taken at ~1 cm apart on the same Cu substrate in sequential order of the distance away from the precursor. The effect of substrate-position is explained elsewhere,[25] where the variation in film density is due to the

combined effects of temperature gradient and gas phase dynamics in the quartz tube. It is remarkable to observe a tremendous increase in the average size of the hexagonal-shape grains (~10.93 $\mu m^2$) with a large reduction in nucleation density of $4.65 \times 10^4$ nuclei $mm^{-2}$ during the initial growth stage (Figure 3b). It is clear that more nucleation occur near or on the Cu grain boundaries, and adjacent domains coalesce together to form larger domains. Figure 3c shows the presence of hexagonal edges between the gaps where multiple hexagonal domains are merged together leading to a formation of a continuous film (Figure 3d). Figure 3e,f shows the magnified SEM images of an almost perfect large isolated hexagonal domain with each sides angled at 120 °, and the area of ~27 $\mu m^2$.

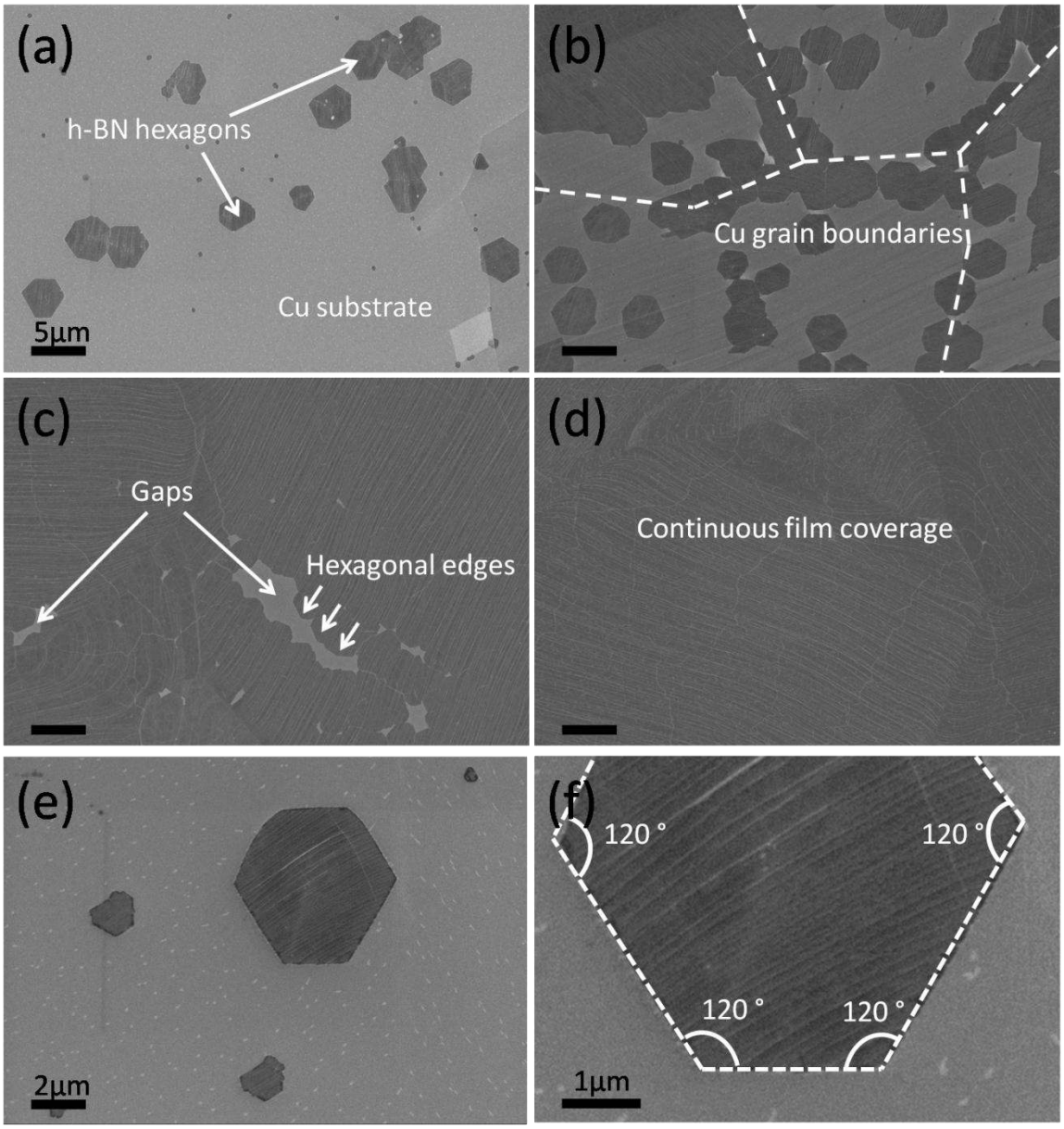


**Figure 3.** Growth process of large hexagonal-shape h-BN domains, from sporadic to continuous film coverage. (a-d) SEM images of the as-grown hexagonal domains on highly polished Cu foils taken at ~1 cm apart in sequential order of the distance from the source, showing a gradual gradient of increasing nucleation density of the hexagonal domains coalesce to form a continuous film. Scale bars, 5 µm. (e,f) Magnified SEM images of a large isolated h-BN hexagons with sides angled at 120 °.

The hexagonal domains were transferred onto $SiO_2$/Si substrate to investigate the morphology and optical properties. Figure 4a shows an optical image of the large hexagonal-shape h-BN domains with enhanced contrast and a relatively weak Raman peak at 1371 $cm^{-1}$ (inset of Figure 4a) corresponding to the $E_{2g}$ vibrational mode of h-BN. The weak intensity of the Raman spectrum results from the atomically thin layer of h-BN.[51] Another inset in Figure 4a shows a Raman map of an individual hexagon, where the bright yellow region indicates a higher intensity between the range of 1360 to 1380 $cm^{-1}$. The intensity is consistent with the $E_{2g}$ mode of an individual hexagon which shows a distinct contrast against $SiO_2$ substrate, and indicates that the h-BN signal is uniform throughout the hexagonal domain. Figure 4b shows an AFM image of another large individual hexagonal domain, clearly depicting a hexagonal shape with a step height of ~1 nm, and an area ~35 $\mu m^2$. White spots on the hexagonal domain are observed due to poly(methyl methacrylate) (PMMA) residues left during the transfer process. The slight increase in AFM thickness measurement for a monolayer h-BN is likely due to the chemical contrast between the h-BN film and the substrate ($SiO_2$).[6, 52] AFM tip have a stronger attraction towards the substrate resulting in an apparently thicker film. This phenomenon had been reported for single-layer graphene measuring up to ~1 nm. For a more credible thickness measurement, transmission electron microscopy (TEM) was utilized. Figure 4c shows the atomic arrangement, and a TEM image taken at the folded edge (inset of Figure 4c) corresponding to a single layer h-BN film and fast Fourier transform (FFT) reveals a distinct hexagonal structure (inset of Figure 4c). X-ray photoelectron spectroscopy (XPS) spectra of B 1s peak and N 1s peak are located at 190.7 and 398.3 eV (Figure 4d,e), respectively. These results are in good agreement with previous reported results.[53, 54] The XPS elemental stoichiometry analysis reveals that the B/N ratio is 1:1.06, signifying an almost equal composition of B and N elements. This also indicates that the configuration of B and N atoms in the film are B-N bonded and further confirms the film's hexagonal structure.

The optical bandgap (OBG), $E_g$, was measured on the transferred h-BN film/quartz substrate by UV-visible spectroscopy. Using a blank quartz substrate as a baseline for the measurements, a strong peak

is observed at 202 nm in the absorption spectrum as shown in Figure 4f. By using the derived formula for direct bandgap semiconductor, the absorption coefficient can be defined as $\alpha = C(E - E_g)^{1/2}/E$,[55] where C is a constant and E is the photon energy. Note that α can be obtained from the optical absorption, *A*, and film thickness *d* (taken as 1 nm) using the relation given by $\alpha = A/d$. To compute the OBG, we plot $(\alpha E)^2$ vs. *E*, in Figure 4g and extrapolate the straight line of the energy dispersion curve to intersect the x-axis (*E*) to obtain the value of $E_g$. Our calculation of $E_g$= 6.04 eV agrees with previous measured values which ranged from 5.84 to 6.07.[3, 26-28] The measured OBG suggests the as-grown h-BN film to be highly transparent and electrically insulating.

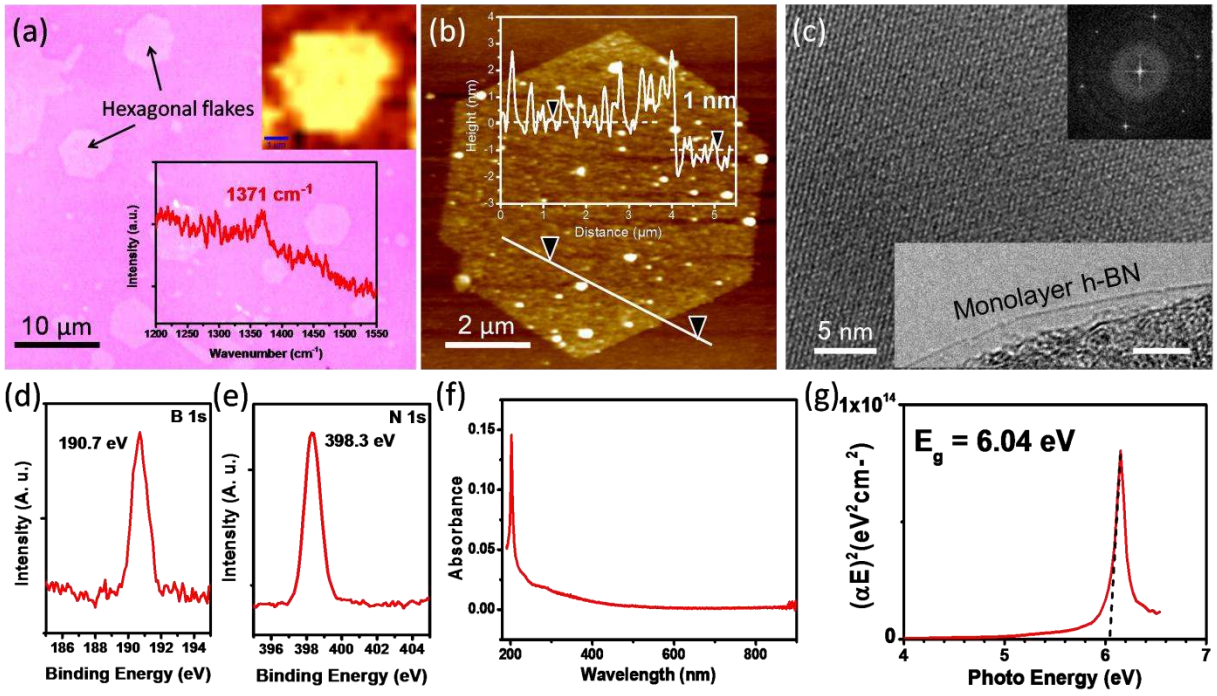


**Figure 4.** Characterization of hexagonal-shape h-BN domains. (a) Optical micrograph of h-BN hexagons on $SiO_2$/Si substrate. The insets are the corresponding Raman spectrum with peak at 1371 $cm^{-1}$ and mapping on a hexagonal domain. Bright yellow region in the Raman map indicates a higher intensity peaks within the range of 1360 to 1380 $cm^{-1}$, corresponding to the $E_{2g}$ vibration mode of h-BN. (b) AFM image with scanned line over the edge of the h-BN domain. The inset shows the height profile of the scanned line with a thickness of 1 nm. (c) Top-view TEM image and image taken at the folded edge

(inset) of a single-layer h-BN film, scale bar 5 nm. The inset FFT reveals a hexagonal crystalline structure. XPS spectra of (d) B 1s, and (e) N 1s with binding energies peaks at 190.7 and 398.3 eV, respectively. (f) UV-Vis absorption spectrum of h-BN film measured at room temperature on quartz substrate, (g) Tauc's plot of $(\alpha E)^2$ vs. $E$ plot for bandgap measurement of h-BN film grown on polished Cu.

A comparison between the h-BN films grown on unpolished and polished Cu substrates was done after the films were transferred onto $SiO_2$/Si substrates. The Optical and AFM images (see Supporting Information Figure S2) revealed a marked contrast between the films. It is observed that the h-BN film grown using polished substrate is thinner (1 nm as compared to 2.2 nm), smoother ($R_q$ of 1.03 nm as compared to 1.62 nm), and more pristine with fewer defects as compared to the film grown using unpolished substrate. Although the Raman peaks at 1370 $cm^{-1}$ are obtained on both films, a slight narrowing of peak is observed on the h-BN film grown using polished Cu, with a calculated full width at half maximum (FHWM) of 19.31 $cm^{-1}$ as compared to 22.74 $cm^{-1}$ for the h-BN film grown using unpolished substrate. This is likely due to the increased in grain size,[56] better crystallinity with lesser defects.

**Discussion**

From previous reports on the influence Cu surface morphology in graphene-growth,[32, 33] it is known that the rough surfaces or presence of impurities, and grain boundaries are likely to act as nucleation seeds, leading to an enhanced rate of nucleation. This is because of a lower effective surface energy for rough surfaces, which diminishes Gibbs free energy barrier and thus, facilitates heterogeneous nucleation.[57] To further elucidate the effect of substrate surface roughness on the growth mechanism of h-BN, we analyze a typical SEM image (Figure 5a) of the nucleation pattern during the initial stage of growth of h-BN domains on an unpolished Cu. It is observed that more nucleation of triangular domains tend to form along deliberately scratched regions (Figure 5b), as well as on the Cu grain boundaries (Figure 5d), while

lesser triangles nucleating away at remote regions of the Cu grains (Figure 5c). The triangular domains also tends to form in a parallel manner,[22] which also correlates to the grooves on the unpolished substrate surface. These Parallel strips of h-BN can be easily observed when the nucleation density is high in the initial stage of growth (see Supporting Information Figure S3). This is the scenario of growth mechanism with unpolished Cu foil. However, unlike the growth on unpolished surface of Cu, growth dynamics may significantly be affected on a polished Cu foil (discussed later).

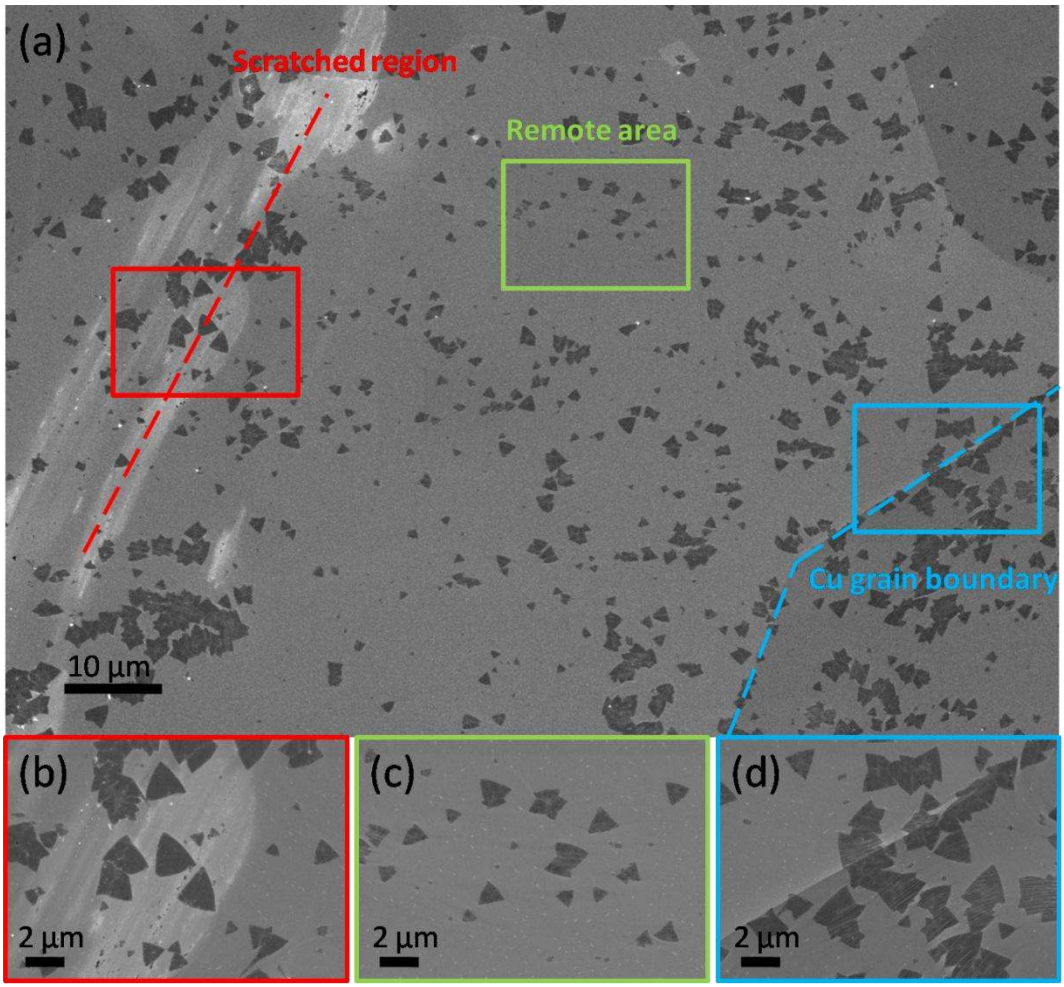


**Figure 5.** Influence of Cu surface morphology on h-BN nucleation. (a) SEM image of initial stage of growth of h-BN on an unpolished Cu foil. Magnified SEM images of (b) scratched region, (c) at a remote area away from Cu grain boundaries, and (d) on a Cu grain boundary.

A recent theoretical modelling on growth of h-BN suggests that triangular-shape h-BN domains result from N-terminated zig-zag edges, which are energetically favoured over B-terminated ones,[47] leading to a triangular shape with all three sides with N-termination as shown in Figure 6a. In order for a hexagonal-shape domain to occur, alternating N and B termination edges must be present as depicted in the schematic of Figure 6b. Since the growth conditions remain the same while only the Cu underwent electropolishing in our procedure, the CVD conditions such as temperature, pressure, and rate of gas flow can be eliminated. XPS measurements were done on both the polished and unpolished Cu substrates which reveal that there is an increase in surface oxygen content on the polished Cu (see Supporting Information Figure S4). During electropolishing, the Cu ions react with phosphoric acid ($H_3PO_4$) electrolyte, and surface oxidation occur in forms of $Cu_2O$, CuO and $Cu(OH)_2$.[58] Therefore, the interaction of the nucleating atoms with the smooth copper surface and higher surface oxygen content must have played a role in reducing the edge-attachment barrier during the growth leading to an energetically favourable N or B edge termination. Due to the smooth Cu surface, a higher effective surface energy is expected to increase Gibbs free energy barrier which restricts nucleation. For nucleation to occur, the activated atoms must surmount the Gibbs free energy barrier, which leads to a more homogenous or suppressed nucleation. The growth of hexagonal-shape 2D h-BN domains follows after the nucleation. Though, an exact mechanism of the formation of hexagonal pattern is not known, a possible explanation is as follows. At temperature 1050 °C and above, borazine ($B_3H_6N_3$) and aminoborane ($BH_2NH_2$) molecules dissociate into BN radicals and diffuse along the Cu surface. The smooth Cu surface effectively reduces the kinetic diffusion barrier and enhances the surface mobility of the free BN radicals, enabling them to have longer diffusion length and move freely along the active edges. In addition, surface oxygen on the Cu is enhanced during electropolishing process. The increased in surface oxidation on Cu facilitates dissociation of the precursor gas and enhances the dehydrogenation process along the edges of the domains.[43] As edge-attachment and lattice integration involves dehydrogenation at domain edges, the edge-attachment barrier is effectively reduced. Hence, the increased Gibbs free energy barrier and enhanced surface diffusivity, due to the smooth surface, suppresses the nucleation and produces

larger h-BN domains. In addition, due to the increase in surface oxygen, the edge-attachment energy barrier is decreased and the energetic BN radicals have sufficient energy to bond onto both N and B-terminated edges, thus forming hexagonal-shape domains. On the other hand, for unpolished Cu substrate, the roughness inhibits the surface diffusivity by trapping BN radicals due to its surface irregularities, restricting the growth and due to the lack of surface oxygen on the Cu, only N-terminated edges are energetically favourable. This results in the formation of triangular shaped h-BN domains.

It is also observed that the hexagonal domains do not always exist in perfect symmetry. Although the shapes are generally hexagonal, some are elongated at one end and shorter at the other (see Supporting Information Figure S5). This phenomenon is expected due to the asymmetric nature of N and B-terminated edges and other growth conditions such as high pressure and gas flow rate. Moreover, such irregular shape hexagonal domains have also been reported for graphene.[35] The hexagonal domains do not have a preferred orientations as they nucleate randomly within a confined Cu grain (see Supporting Information Figure S6) which is also the case in triangular h-BN. As the Cu substrate undergoes high temperature annealing during h-BN growth, it predominantly reconstructs into (100) surface orientation (see Supporting Information Figure S7) Therefore, h-BN does not grow epitaxially on the Cu surface due to the mismatch between a four-fold symmetry of the (100) Cu surface and the six-fold symmetry of the h-BN domains. This leads to more rotational orientations of the h-BN domains.

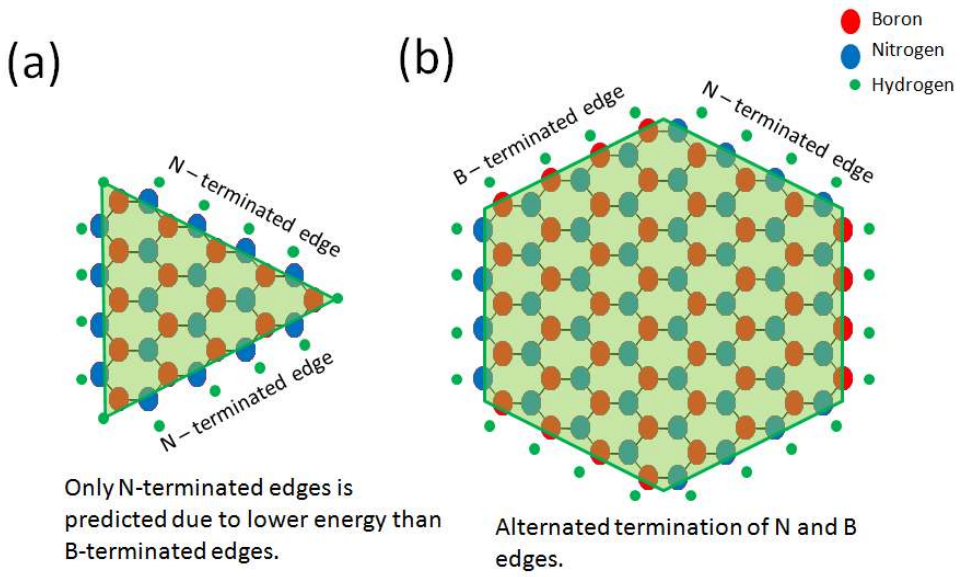


**Figure 6.** Geometric comparison of atoms arrangement on a monolayer triangular and hexagonal-shape h-BN domains. (a) Triangular structure with all sides with N-terminated edges, and (b) hexagonal structure with alternating N and B-terminated edges.

In conclusion, we have successfully synthesized very large (~35 $\mu m^2$) crystalline monolayer h-BN hexagons using highly smoothened polished Cu substrate. We observed that the nucleation density and domain sizes are highly dependent on the surface morphology and oxygen content of the Cu substrate. Due to the smooth Cu surface, nucleation is impeded as a result of the rise in Gibbs energy barrier[57] while the enhanced surface diffusivity of the BN radicals increases the lateral growth of the 2D islands. In addition, due to increased surface oxygen in the Cu, the edge-attachment energy barrier is reduce and the active BN radicals become energetically favourable to bond on both N and B-terminated edges. With a combination of suppressed nucleation, enhanced lateral growth rate, and ability to bind onto edges regardless of N or B-termination, large hexagonal-shape domains can be obtained. By achieving larger h-BN domains, the grain boundaries-induced defects are effectively reduced, and a smoother and higher quality film is achieved. Furthermore, similar to graphene, hexagonal-shape h-BN domains can be used as a prelude for ultra-large domains. Our ability to achieve large single-crystal h-BN domains is vital for scalable high-performance graphene devices as most of the present works are limited to using

exfoliated h-BN flakes. Thus, this finding opens up the possibility of integrating multiple graphene-based devices onto a single sheet of crystalline h-BN substrate.

## ASSOCIATED CONTENT

### Supporting Information

Methods details and Figures S1-S7. This material is available free of charge via the Internet at http://pubs.acs.org.

## AUTHOR INFORMATION

### Corresponding author

*Email: HTTEO@ntu.edu.sg

## ACKNOWLEDGEMENTS

The authors acknowledge the support from MINDEF Singapore and Army Research Laboratory (ARL) USA. We are thankful to Dr. Eric Wetzel, Dr. Raymond Mackay, and Dr. Kristopher Behler of the U.S. Army Research Lab for their aid and input in the Cu surface morphology evaluation.

REFERENCES


1. Tao, O.; Yuanping, C.; Yuee, X.; Kaike, Y.; Zhigang, B.; Jianxin, Z. *Nanotechnology* **2010,** 21, (24), 245701 (6 pp.).
2. Balandin, A. A. *Nature Materials* **2011,** 10, (8), 569-581.
3. Song, L.; Ci, L.; Lu, H.; Sorokin, P. B.; Jin, C.; Ni, J.; Kvashnin, A. G.; Kvashnin, D. G.; Lou, J.; Yakobson, B. I.; Ajayan, P. M. *Nano Letters* **2010,** 10, (8), 3209-3215.
4. Changgu, L.; Xiaoding, W.; Kysar, J. W.; Hone, J. *Science* **2008,** 321, (5887), 385-8.
5. Watanabe, K.; Taniguchi, T.; Kanda, H. *Nature Materials* **2004,** 3, (6), 404-409.
6. Novoselov, K. S.; Geim, A. K.; Morozov, S. V.; Jiang, D.; Zhang, Y.; Dubonos, S. V.; Grigorieva, I. V.; Firsov, A. A. *Science* **2004,** 306, (5696), 666-9.
7. Xuesong, L.; Weiwei, C.; Jinho, A.; Seyoung, K.; Junghyo, N.; Dongxing, Y.; Piner, R.; Velamakanni, A.; Inhwa, J.; Tutuc, E.; Banerjee, S. K.; Colombo, L.; Ruoff, R. S. *Science* **2009,** 324, (5932), 1312-14.
8. Liu, Z.; Ma, L.; Shi, G.; Zhou, W.; Gong, Y.; Lei, S.; Yang, X.; Zhang, J.; Yu, J.; Hackenberg, K. P.; Babakhani, A.; Idrobo, J.-C.; Vajtai, R.; Lou, J.; Ajayan, P. M. *Nat Nano* **2013,** 8, (2), 119-124.
9. Levendorf, M. P.; Kim, C.-J.; Brown, L.; Huang, P. Y.; Havener, R. W.; Muller, D. A.; Park, J. *Nature* **2012,** 488, (7413), 627-632.
10. Dean, C. R.; Young, A. F.; Meric, I.; Lee, C.; Wang, L.; Sorgenfrei, S.; Watanabe, K.; Taniguchi, T.; Kim, P.; Shepard, K. L.; Hone, J. *Nature Nanotechnology* **2010,** 5, (10), 722-6.
11. Lee, K. H.; Shin, H.-J.; Lee, J.; Lee, I.-Y.; Kim, G.-H.; Choi, J.-Y.; Kim, S.-W. *Nano Letters* **2012,** 12, (2), 714-718.
12. Han, W.; Taychatanapat, T.; Hsu, A.; Watanabe, K.; Taniguchi, T.; Jarillo-Herrero, P.; Palacios, T. *IEEE Electron Device Letters* **2011,** 32, (9), 1209-11.
13. Britnell, L.; Gorbachev, R. V.; Jalil, R.; Belle, B. D.; Schedin, F.; Mishchenko, A.; Georgiou, T.; Katsnelson, M. I.; Eaves, L.; Morozov, S. V.; Peres, N. M. R.; Leist, J.; Geim, A. K.; Novoselov, K. S.; Ponomarenko, L. A. *Science* **2012,** 335, (6071), 947-50.
14. Özçelik, V. O.; Ciraci, S. *The Journal of Physical Chemistry C* **2013,** 117, (29), 15327-15334.
15. Lipp, A.; Schwetz, K. A.; Hunold, K. *Journal of the European Ceramic Society* **1989,** 5, (1), 3-9.
16. Salvatore, G. A.; Münzenrieder, N.; Barraud, C.; Petti, L.; Zysset, C.; Büthe, L.; Ensslin, K.; Troester, G. *ACS Nano* **2013**.
17. Watanabe, K.; Taniguchi, T.; Niiyama, T.; Miya, K.; Taniguchi, M. *Nat Photon* **2009,** 3, (10), 591-594.
18. Fujihara, T.; Cho, H.-B.; Nakayama, T.; Suzuki, T.; Jiang, W.; Suematsu, H.; Kim, H. D.; Niihara, K. *Journal of the American Ceramic Society* **2012,** 95, (1), 369-373.
19. Husain, E.; Narayanan, T. N.; Taha-Tijerina, J. J.; Vinod, S.; Vajtai, R.; Ajayan, P. M. *ACS Applied Materials and Interfaces* **2013,** 5, (10), 4129-4135.
20. Liu, Z.; Gong, Y.; Zhou, W.; Ma, L.; Yu, J.; Idrobo, J. C.; Jung, J.; MacDonald, A. H.; Vajtai, R.; Lou, J.; Ajayan, P. M. *Nat Commun* **2013,** 4.
21. Lei, W.; Portehault, D.; Liu, D.; Qin, S.; Chen, Y. *Nat Commun* **2013,** 4, 1777.
22. Kim, K. K.; Hsu, A.; Jia, X.; Kim, S. M.; Shi, Y.; Hofmann, M.; Nezich, D.; Rodriguez-Nieva, J. F.; Dresselhaus, M.; Palacios, T.; Kong, J. *Nano Letters* **2012,** 12, (1), 161-166.
23. Guo, N.; Wei, J.; Fan, L.; Jia, Y.; Liang, D.; Zhu, H.; Wang, K.; Wu, D. *Nanotechnology* **2012,** 23, (41).
24. Suzuki, S.; Hibino, H. In *Chemical vapor deposition of hexagonal boron nitride*, Hongo Corporation 402, 2-40-13 Hongo, Bunkyo-ku, Tokyo, 113-0033, Japan, 2012; Surface Science Society of Japan: Hongo Corporation 402, 2-40-13 Hongo, Bunkyo-ku, Tokyo, 113-0033, Japan, 2012; pp 133-138.
25. Tay, R. Y.; Wang, X.; Tsang, S. H.; Loh, G. C.; Singh, R. S.; Li, H.; Mallick, G.; Teo, E. *Journal of Materials Chemistry C* **2013**.

26. Shi, Y.; Hamsen, C.; Jia, X.; Kim, K. K.; Reina, A.; Hofmann, M.; Hsu, A. L.; Zhang, K.; Li, H.; Juang, Z.-Y.; Dresselhaus, M. S.; Li, L.-J.; Kong, J. *Nano Letters* **2010,** 10, (10), 4134-4139.
27. Gao, Y.; Ren, W.; Ma, T.; Liu, Z.; Zhang, Y.; Liu, W.-B.; Ma, L.-P.; Ma, X.; Cheng, H.-M. *ACS Nano* **2013**.
28. Kim, G.; Jang, A. R.; Jeong, H. Y.; Lee, Z.; Kang, D. J.; Shin, H. S. *Nano Letters* **2013,** 13, (4), 1834-1839.
29. Gibb, A. L.; Alem, N.; Chen, J.-H.; Erickson, K. J.; Ciston, J.; Gautam, A.; Linck, M.; Zettl, A. *Journal of the American Chemical Society* **2013,** 135, (18), 6758-6761.
30. Zhou, H.; Yu, W. J.; Liu, L.; Cheng, R.; Chen, Y.; Huang, X.; Liu, Y.; Wang, Y.; Huang, Y.; Duan, X. *Nat Commun* **2013,** 4.
31. Wu, T.; Ding, G.; Shen, H.; Wang, H.; Sun, L.; Jiang, D.; Xie, X.; Jiang, M. *Advanced Functional Materials* **2013,** 23, (2), 198-203.
32. Han, G. H.; Gunes, F.; Bae, J. J.; Kim, E. S.; Chae, S. J.; Shin, H.-J.; Choi, J.-Y.; Pribat, D.; Lee, Y. H. *Nano Letters* **2011,** 11, (10), 4144-4148.
33. Luo, Z.; Lu, Y.; Singer, D. W.; Berck, M. E.; Somers, L. A.; Goldsmith, B. R.; Johnson, A. T. C. *Chemistry of Materials* **2011,** 23, (6), 1441-1447.
34. Mohsin, A.; Liu, L.; Liu, P.; Deng, W.; Ivanov, I. N.; Li, G.; Dyck, O. E.; Duscher, G.; Dunlap, J. R.; Xiao, K.; Gu, G. *ACS Nano* **2013,** 7, (10), 8924-8931.
35. Luo, Z.; Kim, S.; Kawamoto, N.; Rappe, A. M.; Johnson, A. T. C. *ACS Nano* **2011,** 5, (11), 9154-9160.
36. Wu, W.; Jauregui, L. A.; Su, Z.; Liu, Z.; Bao, J.; Chen, Y. P.; Yu, Q. *Advanced Materials* **2011,** 23, (42), 4898-4903.
37. Wang, H.; Wang, G.; Bao, P.; Yang, S.; Zhu, W.; Xie, X.; Zhang, W.-J. *Journal of the American Chemical Society* **2012,** 134, (8), 3627-3630.
38. Wu, Y. A.; Robertson, A. W.; Schaffel, F.; Speller, S. C.; Warner, J. H. *Chemistry of Materials* **2011,** 23, (20), 4543-4547.
39. Liu, W.; Li, H.; Xu, C.; Khatami, Y.; Banerjee, K. *Carbon* **2011,** 49, (13), 4122-4130.
40. Xue, J.; Sanchez-Yamagishi, J.; Bulmash, D.; Jacquod, P.; Deshpande, A.; Watanabe, K.; Taniguchi, T.; Jarillo-Herrero, P.; LeRoy, B. J. *Nat Mater* **2011,** 10, (4), 282-285.
41. Zhang, Y.; Zhang, L.; Kim, P.; Ge, M.; Li, Z.; Zhou, C. *Nano Letters* **2012,** 12, (6), 2810-2816.
42. Meca, E.; Lowengrub, J.; Kim, H.; Mattevi, C.; Shenoy, V. B. *Nano Letters* **2013**.
43. Hao, Y.; Bharathi, M. S.; Wang, L.; Liu, Y.; Chen, H.; Nie, S.; Wang, X.; Chou, H.; Tan, C.; Fallahazad, B.; Ramanarayan, H.; Magnuson, C. W.; Tutuc, E.; Yakobson, B. I.; McCarty, K. F.; Zhang, Y.-W.; Kim, P.; Hone, J.; Colombo, L.; Ruoff, R. S. *Science* **2013,** 342, (6159), 720-723.
44. han, g. h.; rodriguez-manzo, j. a.; Lee, C.-W.; kybert, n. j.; Lerner, M. B.; qi, z. j.; dattoli, e. n.; Rappe, A. M.; Drndic, M.; Johnson, A. T. C. *ACS Nano* **2013**.
45. Zhao, Z.; Yang, Z.; Wen, Y.; Wang, Y. *Journal of the American Ceramic Society* **2011,** 94, (12), 4496-4501.
46. Li, M.; Xu, L.; Sun, C.; Ju, Z.; Qian, Y. *Journal of Materials Chemistry* **2009,** 19, (43), 8086-8091.
47. Liu, Y.; Bhowmick, S.; Yakobson, B. I. *Nano Letters* **2011,** 11, (8), 3113-3116.
48. Hirsch, J.; Lucke, K. *Acta Metallurgica* **1988,** 36, (11), 2863-82.
49. Baitalow, F.; Wolf, G.; Grolier, J. P. E.; Dan, F.; Randzio, S. L. *Thermochimica Acta* **2006,** 445, (2), 121-125.
50. Baumann, J.; Baitalow, F.; Wolf, G. *Thermochimica Acta* **2005,** 430, (1-2), 9-14.
51. Gorbachev, R. V.; Riaz, I.; Nair, R. R.; Jalil, R.; Britnell, L.; Belle, B. D.; Hill, E. W.; Novoselov, K. S.; Watanabe, K.; Taniguchi, T.; Geim, A. K.; Blake, P. *Small* **2011,** 7, (4), 465-8.
52. Ferrari, A. C.; Meyer, J. C.; Scardaci, V.; Casiraghi, C.; Lazzeri, M.; Mauri, F.; Piscanec, S.; Jiang, D.; Novoselov, K. S.; Roth, S.; Geim, A. K. *Physical Review Letters* **2006,** 97, (18).
53. Trehan, R.; Lifshitz, Y.; Rabalais, J. W. *Journal of Vacuum Science & Technology A (Vacuum, Surfaces, and Films)* **1990,** 8, (6), 4026-32.

54. Park, K. S.; Lee, D. Y.; Kim, K. J.; Moon, D. W. *Applied Physics Letters* **1997,** 70, (3), 315-17.
55. Yuzuriha, T. H.; Hess, D. W. *Thin Solid Films* **1986,** 140, (2), 199-207.
56. Nemanich, R. J.; Solin, S. A.; Martin, R. M. *Physical Review B (Condensed Matter)* **1981,** 23, (12), 6348-56.
57. *Kinetic theory of liquids*. The Clarendon Press: Oxford, England, 1946; p 488.
58. Kung, T.-M.; Huang, M. R.-S.; Tsao, J.-C.; Liu, C.-P.; Wang, Y.-L. *Journal of Nanoscience and Nanotechnology* **2010,** 10, (11), 7065-7069.